IJMSIT

International Journal of Multidisciplinary Studies and Innovative Technologies

Volume : 1
Number: 1
Year: 2017
Pages: 29 - 35

The Effect of Cold Rolling on Mechanical Properties of Zircaloy-4†

Semih Ağca[1*], Güven Çankaya[2]

[1,2]*Department of Metallurgical and Materials Engineering, Ankara Yıldırım Beyazıt University, Turkey*
[*]*Corresponding author: agcasemih@gmail.com*

Abstract – In this study, Zircaloy-4 rods are heat treated and cold rolled to different (15%, 30%, 45%, 60%, and 75%) reduction ratios to determine the effect of heat treatment and cold rolling on micro and nano scale mechanical properties of Zircaloy-4. Micro scale mechanical properties are investigated by micro Vickers hardness tester and nano scale mechanical properties are studied by universal mechanical tester (UMT). Fracture surfaces of samples are illustrated by scanning electron microscope (SEM). Microstructure of samples are evaluated by optical microscope. It is found that hardness increased with increasing cold rolling reduction ratio both in micro and nano scale. Nano scale measurements showed that the elastic modulus is increased with increasing reduction ratio. Increase in hardness and elastic modulus altered the fracture from ductile to brittle. Fracture mode for samples are determined as mixed mode.

Keywords – Zircaloy-4, UMT, cold rolling, mechanical properties.

I. Introduction

Zirconium alloys are very important for nuclear industry with their outstanding features [1]. Due to enhanced mechanical and physical properties, Zircaloy-4 is the most popular zirconium alloy. Cold rolling is used by many researchers for enhancing the mechanical properties of Zircaloy-4. Fuloria et al. [2] have studied the effect of cold rolling on the hardness and tensile strength of Zircaloy-4. They found that the cold rolling increases the hardness and strength due to increasing of dislocation density and grain refinement. They also found that dislocation density increased with increasing stacking fault probability. Lim et al. [3] have studied the effect of cold rolling and heat treatment on the mechanical properties of Zircaloy-4. It is claimed that texture was developed with higher rolling reduction and it was influenced by final heat treatment. It is also reported that the direction of the test affected the creep strain. Busser et al. [4] have investigated mechanical properties and oxide layer damage evolution in Zircaloy-4 by ring compression test technique. They found that the ring compression test technique has an important potential for both analyzing the mechanical properties of irradiated and non-irradiated nuclear fuel rod cladding materials. Although zirconium alloys are produced by many techniques, cold rolling has been chosen for this study owing to its ease of use and cheapness.

II. Materials and Method

A. Materials

Zircaloy-4 rod with 10 mm diameter is provided from Nanografi Nanotechnology Ltd. Chemical composition of Zircaloy-4 rod is shown in Table 1.

Table 1. Chemical composition of Zircaloy-4 rod

Element	O	CR	Sn	Fe	Zr
Weight	0.16	0.13	1.7	0.24	Balance

B. Sample Preparation

The production processes and the names of Zircaloy-4 samples are shown in Table 2.

Table 2. Chemical composition of Zircaloy-4 rod

Sample name	**Annealing (ºC)**	**Cold rolling (%)**
AR	-	-
AN	700	-
CR15	700	15
CR30	700	30
CR45	700	45
CR60	700	60
CR75	700	75

AR is as-received material. AN is only annealed and other samples are cold rolled to different reduction ratios. The annealing process is performed by an atmosphere controlled heat treatment furnace. The air in the furnace is removed by a vacuum pump with 60 mbar vacuum before filling the atmosphere of the furnace with argon. AN, CR15, CR30, CR45, CR60, and CR75 are annealed by applying 4 hours recrystallization heat treatment at 700ºC in argon atmosphere. Samples are cooled to room temperature in the furnace. CR15, CR30, CR45, CR60, and CR75 are heated to 300ºC in air atmosphere before each pass of cold rolling. These samples are cold rolled by two rolling mills with 240 mm diameter at 1.25 rpm rolling speed. 15% reduction ratio is practiced in each pass. Thereby, 1 pass for CR15, 2 passes for CR30, 3 passes for CR45, 4 passes for CR60, and 5 passes for CR75 are performed. All samples are sectioned both from rolling direction (RD) and transverse direction (TD) to illustrate the anisotropy in the mechanical properties. Sectioned samples mounted into bakelite by a hot mounting press. After hot mounting, mounted samples are grinded with 320, 600, 800, 1000, 1200, 2000, and 2500 grit SiC coated abrasive grinding papers. After this, samples are polished with 6 µm, 3 µm, and 1 µm diamond suspension on flocked polishing cloth.

† This is an extended version of a conference paper (ISMSIT2017).

Polished samples are etched with proper etchant for thirty seconds to reveal the microstructure clearly. Chemical composition of etchant is shown in Table 3.

Table 3. Chemical composition of etchant

Component	Weight(%)
Hydrofluoric acid (HF)	10
Nitric acid (HNO3)	45
Distilled water	45

Transverse (left) and rolling (right) directions of samples are hot mounted to same bakelite as shown in Fig. 1.

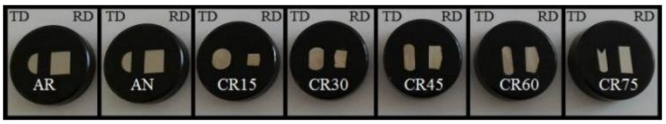

Fig. 1 Prepared samples

C. Micro and Nano Scale Mechanical Tests

Micro scale mechanical properties are examined with SHIMADZU HMV-G micro Vickers hardness tester shown in Fig. 2. Microhardness test is practiced both just after cold rolling process and after polishing and etching. Microhardness measurements are practiced under 9.807 N load and 6 seconds holding time by diamond pyramid indenter.

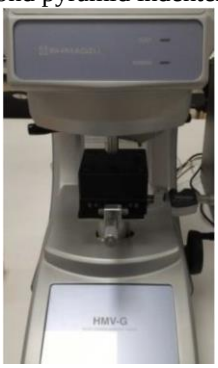

Fig. 2 SHIMADZU HMV-G micro Vickers hardness tester

Nano scale mechanical properties are studied by BRUKER UMT via nanoindentation test mode. UMT is shown in Fig. 3. Rolling and transverse directions of samples are investigated after polishing and etching. Nanoindentation tests are carried out by berkovich diamond triangular pyramid indenter with 100 nm tip radius. Multiple-stage loading profile (from 50 mN to 400 mN with 50 mN increase in each step) is applied to each sample.

Fig. 3 BRUKER UMT

D. Microscopic Examination

Microstructure photographs of etched samples are taken by NIKON Eclipse MA100 inverted optical microscope in 1000X magnification to illustrate the grain structure, orientation, and size.

Fracture surface pictures of samples are taken by FEI Quanta Feg 450 SEM. Scanning is performed in 1000X and 5000X magnification with high vacuum mode. Scanned areas of fracture surfaces are chosen randomly.

III. RESULTS

A. Micro and Nano Scale Mechanical Test Results

Microhardness test is performed both just after cold rolling process and after polishing and etching. The measurements after cold rolling illustrated the effect of cold rolling process on microhardness. On the other hand, micro Vickers hardness test after etching showed the effect of polishing and etching on microhardness. Microhardness values of samples after cold rolling are shown in Fig. 4.

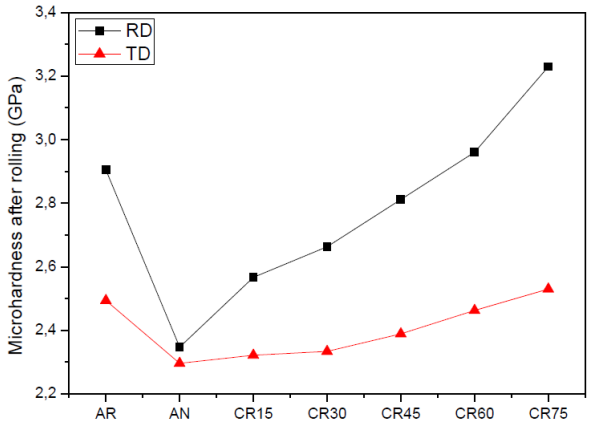

Fig. 4 Microhardness values of samples after cold rolling

AR, AN, CR15, CR30, CR45, CR60, and CR75 after rolling are 2.905, 2.347, 2.567, 2.663, 2.812, 2.961, 3.230 GPa, and 2.494, 2.296, 2.322, 2.334, 2.389, 2.463, 2.530 GPa, respectively. Microhardness value of samples increased with increasing cold rolling reduction ratio in both rolling and transverse directions. Microhardness values of samples after etching are shown in Fig. 5.

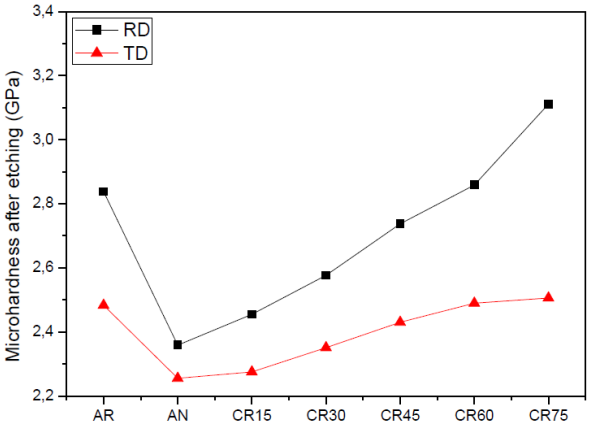

Fig. 5 Microhardness values of samples after etching

Microhardness values of rolling and transverse direction of AR, AN, CR15, CR30, CR45, CR60, and CR75 after etching are 2.838, 2.359, 2.455, 2.577, 2.738, 2.859, 3.112 GPa, and 2.483, 2.255, 2.275, 2.351, 2.43, 2.490, 2.506 GPa, respectively.

Nanoindentation results are represented by illustrating the graphs about the effect of multiple-stage loading on depth of indentation mark. Load-depth graphs of rolling directions of samples are shown in Fig. 6.

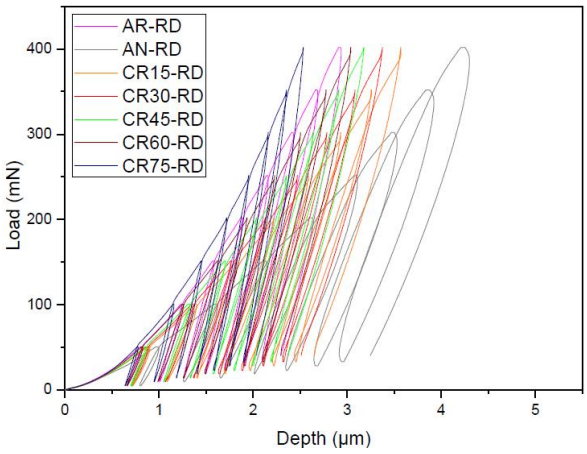

Fig. 6 Load-depth graphs of rolling directions of samples

Steeper slope of the curve means higher elastic modulus and lower depth means higher hardness due to small projected area [7]. CR75 has the highest hardness with minimum depth, and highest elastic modulus with steepest slope of curve. Conversely, AN has the lowest hardness and elastic modulus. Other samples took place according to their reduction ratios. Load-depth graphs of transverse directions of samples are shown in Fig. 7.

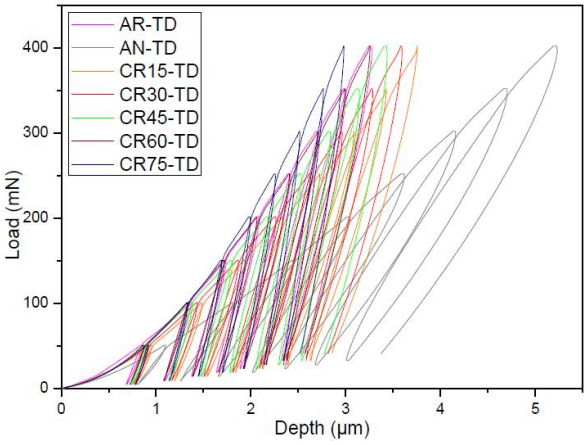

Fig. 7. Load-depth graphs of transverse directions of samples

The gradation of curves in transverse direction is similar to that in rolling direction. CR75 is the hardest sample with having the highest elastic modulus, and vice versa is valid for AN. The shifting of the curves to the left side continued up to curves of CR75 both in rolling and transverse directions. Average nanohardness values of samples after etching are shown in Fig. 8.

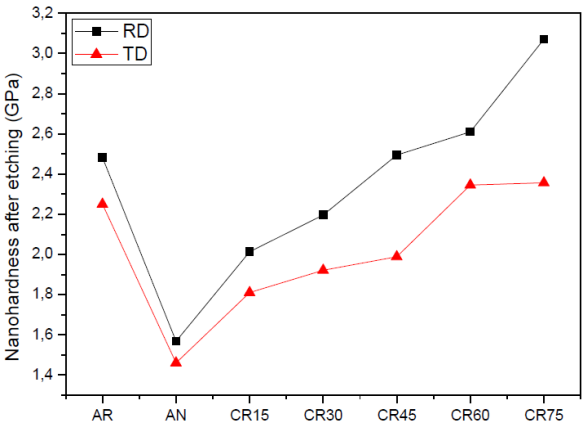

Fig. 8. Average nanohardness values of samples after etching

As seen in Fig. 8, nanohardness increased with increasing of cold rolling reduction ratio as expected. Nanohardness values of rolling direction and transverse direction of AR, AN, CR15, CR30, CR45, CR60, and CR75 after etching are 2.482, 1.568, 2.013, 2.196, 2.494, 2.610, 3.071 GPa, and 2.250, 1.460, 1.810, 1.921, 1.989, 2.345, 2.356 GPa, respectively. Nanohardness values of AR in both directions are similar to those of CR60. The average elastic modulus values of samples are shown in Fig. 9.

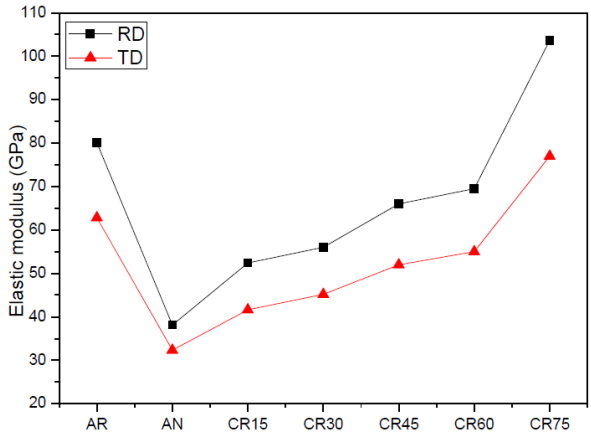

Fig. 9. Average elastic modulus values of samples

As can be seen in Fig. 9, elastic modulus, nanohardness, and microhardness values are interrelated. Elastic modulus values of rolling direction and transverse direction of AR, AN, CR15, CR30, CR45, CR60, and CR75 are 80.1, 38.1, 52.4, 56, 66, 69.5, 103.7 GPa, and 62.8, 32.3, 41.6, 45.2, 52, 55, 77 GPa, respectively.

Elastic modulus values increased with increasing cold rolling reduction ratio. Moreover, elastic modulus values of AR are between CR60 and CR75.

B. Microscopic Examination Results

All samples are etched, and microstructure photographs are taken by inverted optical microscope in 1000X magnification to illustrate the grain structure, orientation, and size. Microstructures of rolling and transverse directions of AR are shown in Fig. 10. The red lines on the photographs represent 20 μm scale bar.

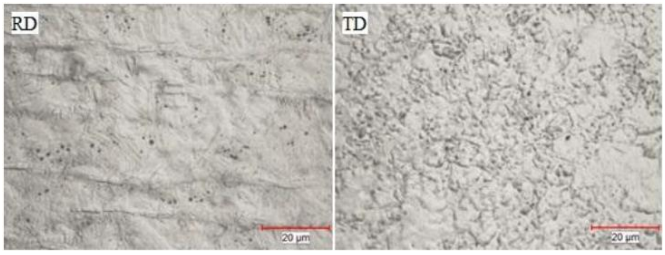

Fig. 10. Microstructures of rolling and transverse directions of AR

As seen in Fig. 10, there are elongated and broken grains in rolling direction. Grain sizes are in the range of 5-15 μm. Rolling direction of sample has bigger grains due to elongation derived from cold rolling. Furthermore, there are some overlong grains in rolling direction. Microstructures of rolling and transverse directions of AN are shown in Fig. 11.

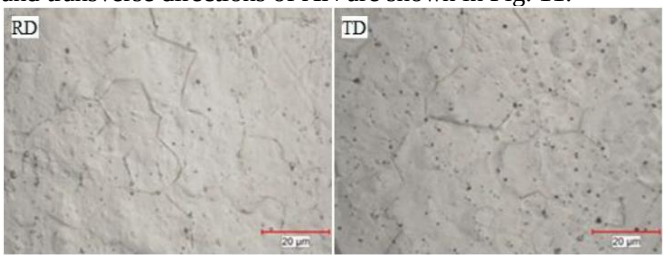

Fig. 11. Microstructures of rolling and transverse directions of AN

As illustrated in Fig. 11, there are equiaxed big grains in both rolling and transverse direction. Grain sizes are in the range of 10-25 μm. Black points on the surface are defects and voids. The orientation could not be seen due to absence of cold rolling process. Fig. 12 shows microstructures of rolling and transverse directions of CR15.

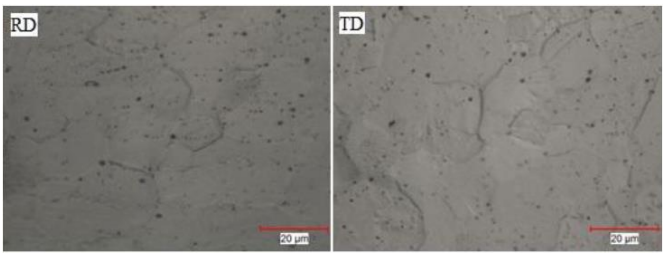

Fig. 12. Microstructures of rolling and transverse directions of CR15

The difference between AN and CR15 is very little. The most notably difference is the alignment of some voids in the rolling direction. In addition, grain size is slightly lower than AN in both directions. Fig. 13 shows microstructures of rolling and transverse directions of CR30.

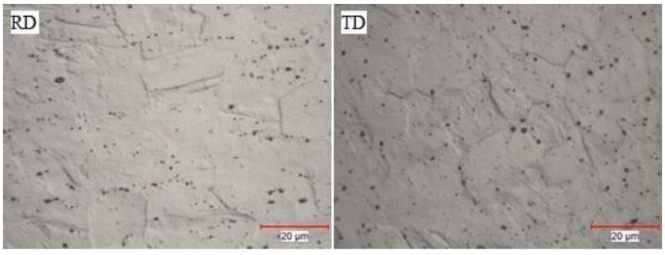

Fig. 13. Microstructures of rolling and transverse directions of CR30

Grains started to elongate in rolling direction, while getting smaller in transverse direction. Grain boundary orientation started to form along the rolling direction. Grain sizes are in the range of 12-20 μm.Fig. 14 shows microstructures of rolling and transverse directions of CR45.

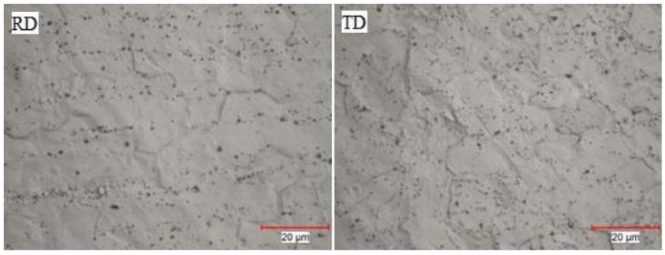

Fig. 14. Microstructures of rolling and transverse directions of CR45

As illustrated in Fig. 14, grain boundary orientation and alignment of voids started to create a band structure in rolling direction. Grains in rolling and transverse directions are smaller than that of CR30. The grain size range is nearly 10-15 μm. The grain sizes in transverse direction are slightly lower than those of rolling direction. Fig. 15 shows microstructures of rolling and transverse directions of CR60.

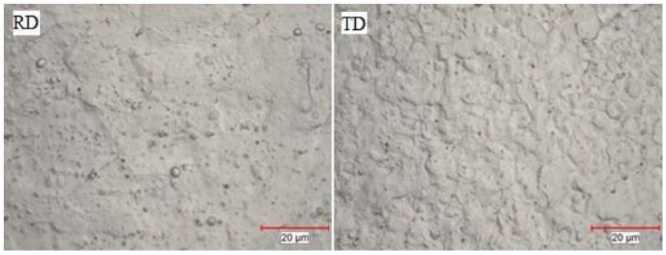

Fig. 15. Microstructures of rolling and transverse directions of CR60

Grain sizes of rolling and transverse directions continue to decreasing. Grain sizes of CR60 are in the range of 5-13 μm. Fig. 16 shows microstructures of rolling and transverse directions of CR75.

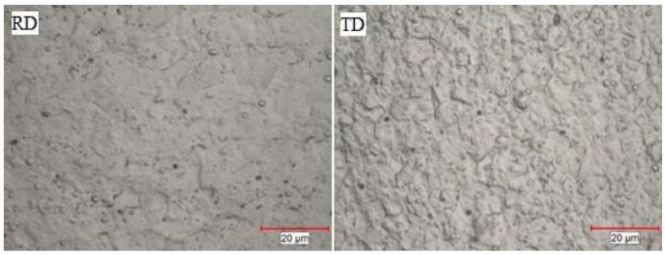

Fig. 16. Microstructures of rolling and transverse directions of CR75

As illustrated in Fig. 16, an orientation formed along the rolling direction. Grain sizes in rolling and transverse directions reached to their minimum values in the range of 3-10 μm. Transverse direction of CR75 has lower grain sizes than rolling direction like other samples. Fig. 17 shows average grain sizes of samples.

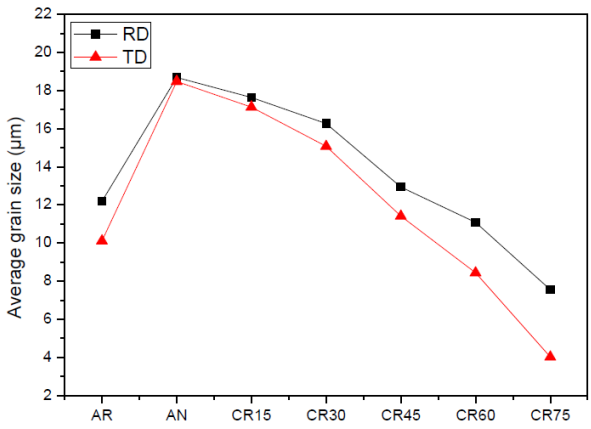

Fig. 17. Average grain sizes of samples

Average grain sizes of rolling direction of AR, AN, CR15, CR30, CR45, CR60, and CR75 are 12.19, 18.68, 17.63, 16.26, 12.93, 11.08, 7.55 μm. Average grain sizes of transverse direction of samples are 10.11, 18.47, 17.12, 15.07, 11.41, 8.43, 4.02 μm, respectively.

Average grain sizes of transverse directions are lower than average grain sizes of rolling directions. In addition, average grain size decreased with increasing of cold rolling reduction ratio. Average grain size values of AR are between CR45 and CR60.

Fracture surface pictures of samples are taken randomly in 1000X and 5000X magnification with high vacuum mode to illustrate fracture behavior of samples. Fig. 18 shows fractography images of AR.

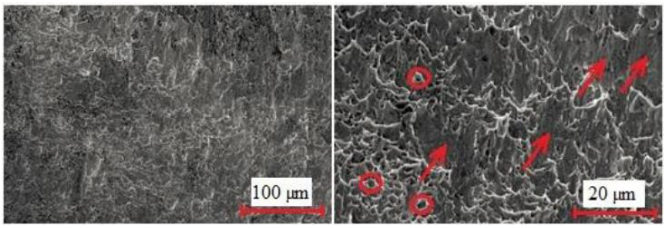

Fig. 18. Fractography images of AR in 1000X (left) & 5000X (right)

Flat areas shown with arrows represent the quasi-cleavage surfaces; on the other hand, small voids shown with circles stand for dimples. As seen in Fig. 18, the amount of quasi-cleavage surfaces is higher than amount of dimples. Consequently, the fracture behavior is mixed fracture mode but it is closer to brittle fracture mode more than ductile fracture mode. Fig. 19 shows fractography images of AN in 1000X and 5000X magnification.

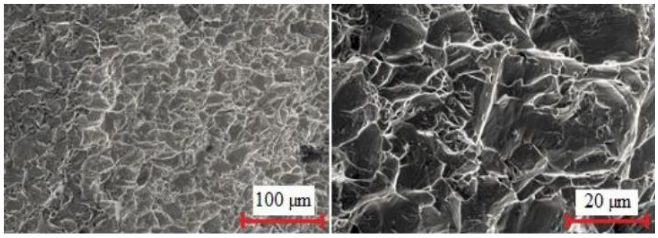

Fig. 19. Fractography images of AN in 1000X (left) & 5000X (right)

There are a lot of big dimples and little quasi-cleavage surfaces, so the fracture behavior is mixed fracture mode but closer to ductile fracture mode. Fig. 20 shows fractography images of CR15 in 1000X and 5000X magnification.

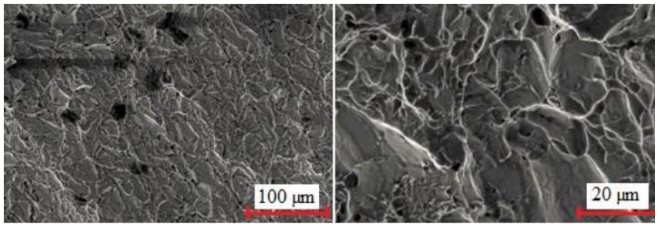

Fig. 20. Fractography images of CR15 in 1000X (left) & 5000X (right)

As seen in Fig. 20, the amount of dimples decreased and quasi-cleavage surfaces increased slightly in comparison with AN. There are big cavities in the fractography image taken in 1000X magnification. These cavities assumed to be voids that formed in fabrication process, because they are too big to consider like a dimple. Fig. 21 shows fractography images of CR30 in 1000X and 5000X magnification.

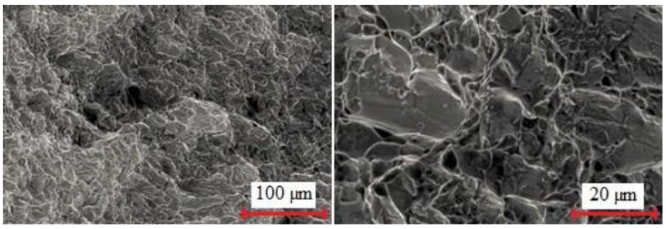

Fig. 21. Fractography images of CR30 in 1000X (left) & 5000X (right)

The amount of dimples continued to decrease and quasi-cleavage surfaces became more dominant when compared with CR15. The elastic modulus and hardness increased with increasing of cold rolling reduction ratio as mentioned before. Therefore, mixed fracture mode became closer to brittle fracture mode. Fig. 22 shows fractography images of CR45 in 1000X and 5000X magnification.

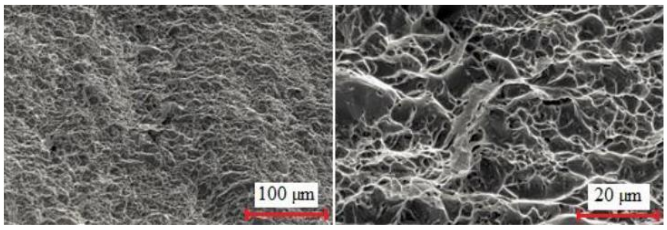

Fig. 22. Fractography images of CR45 in 1000X (left) & 5000X (right)

As seen in Fig. 22, there is an obvious superiority of quasi-cleavage surfaces on dimples. This situation is related with high elastic modulus and hardness. Fig. 23 shows fractography images of CR60 in 1000X and 5000X magnification.

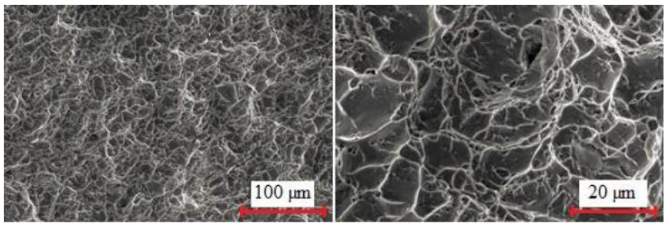

Fig. 23. Fractography images of CR60 in 1000X (left) & 5000X (right)

The amount of dimples continued to decrease; conversely, the amount of quasi-cleavage surfaces continued to increase. Moreover, the surface is smoother than that of CR45. Fig. 24 shows fractography images of CR75 in 1000X and 5000X magnification.

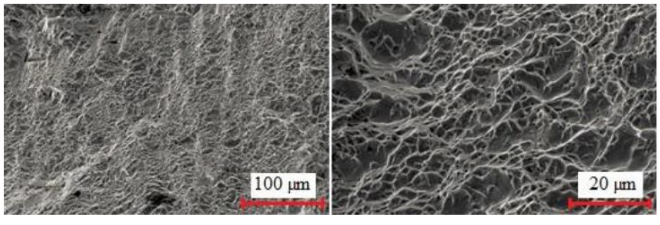

Fig. 24. Fractography images of CR75 in 1000X (left) & 5000X (right)

As illustrated in Fig. 24, the amount of quasi-cleavage surfaces reached to maximum in comparison with other samples. On the other hand, the amount of dimples is very little. As a result, AN is the most ductile, and CR75 is the most brittle sample.

IV. DISCUSSION

Grain refinement and work hardening are main mechanisms for microhardness increment [2]. It can be understood from Fig. 4 that microhardness values of rolling direction of samples are higher than that of transverse direction of samples after cold rolling process. The reason for this is the grain orientation difference between two directions. The anisotropy of mechanical properties in materials with longitudinal grains is a well-known fact [5]. It also can be seen in Figure 3.21 that the distance between microhardness value of rolling direction and microhardness value of transverse direction increased with increasing cold rolling reduction ratio. The evolution in grain refinement and work hardening mechanisms is the reason for increment in the distance between microhardness value of rolling direction and that of transverse direction. Work hardening mechanism in rolling direction is more effective than that in transverse direction, and its effect increases with increasing reduction ratio. On the other hand, grain refinement mechanisms in both directions are similar. The direction-dependent change of work hardening mechanism is the main factor for this situation [2].

If Fig. 4 and Fig. 5 are analysed together, it can be seen that polishing and etching have very little reducing effect on microhardness values of samples in both rolling and transverse directions. This situation reveals the relationship between surface roughness and hardness. As it is known, hardness increases with decreasing of surface roughness [6]. Etching slightly increased the surface roughness and thus reduced the hardness.

As can be seen in Fig. 6 and Fig. 7, the slopes of load-depth curves of rolling directions are steeper than those of transverse directions. Furthermore, maximum depth values of transverse directions are higher than those of rolling directions. Consequently, elastic modulus and hardness values of rolling directions of samples are higher than those of transverse directions of samples. This result is in a good agreement with the information mentioned before in microhardness values.

The homogeneity of samples can be explained with shape of the curves. If the curves of different loads (from 50 mN to 400 mN) form a regular line, it means that the sample is homogeneous. Load-depth figures of samples illustrate that the homogeneity of all samples are in a good level [8].

The nose of the curve is sharper in samples with high elastic modulus, and more cambered in samples with low elastic modulus. Internal stresses play an important role in this situation by influencing the recovery behaviour [9].

Average nanohardness values of samples are in a good agreement with microhardness values and load-depth curves. Also, these values are in corroboration with the literature [10, 11].

Mechanical properties of AR and CR60 are very similar. The well known production route for rod shaped materials includes hot extrusion, multiple cold rolling, and annealing [12]. It is predicted that AR cold rolled to approximately 60% reduction ratio during fabrication.

The overlong grains are not typical for cold rolled materials, and can be seen in hot rolled samples. The overlong grains should be derived from the hot rolling part of production route of AR.

The hardness increased with decreasing of grain size in rolling direction. For example, CR75-RD is harder than CR60-RD by having smaller grains. On the other hand, CR75-RD is harder than CR75-TD but grains of CR75-TD are smaller. the mechanisms for increasing of hardness are grain refinement and work hardening. The work hardening mechanism is more effective in rolling direction. In addition, the anisotropy due to grain orientation affects the hardness. The effects of work hardening and grain orientation are more dominant than grain refinement effect. Consequently, higher hardness of CR75-RD from CR75-TD becomes reasonable, although grains of CR75-RD are bigger.

Cleavage surfaces are characteristic for brittle materials, and dimples are characteristic for ductile materials. Furthermore, cleavage surfaces and dimples can be located together in most of the metals, and this situation is named mixed fracture mode [13, 14]. It can be concluded that the fracture behavior of samples changed with cold rolling. AN is the most ductile sample with maximum amount of dimples and CR75 is the most brittle sample with maximum amount of quasi-cleavage surfaces.

V. CONCLUSION

Microhardness values of samples increased with increasing cold rolling reduction ratio in both rolling and transverse directions by grain refinement and work hardening mechanisms in microscale. In addition, work hardening mechanism in rolling direction is more effective than that in transverse direction, and its effect increases with increasing reduction ratio. On the other hand, grain refinement mechanisms in both directions are similar. Furthermore, polishing and etching have very little reducing effect on microhardness values of samples in both rolling and transverse directions.

Nanohardness and elastic modulus increased with increasing of cold rolling reduction ratio. Moreover, elastic modulus and hardness values of rolling direction of samples are higher than that of transverse direction of samples. Load-depth figures of samples illustrate that the homogeneity of all samples are in a good level.

The hardness increased with decreasing of grain size in rolling direction. In addition, average grain sizes of transverse directions are lower than average grain sizes of rolling directions. Samples have mixed fracture mode with quasi-cleavage surfaces and dimples. The fracture behaviour of samples altered from ductile to brittle with increasing of cold rolling reduction ratio.

ACKNOWLEDGMENT

The authors would like to thank Assoc. Prof. Dr. Çağrı ÇIRAK, Res. Assist. Dr. Fikret YILMAZ, Bayram BAYAR, Abdülaziz GÜNEŞ and Harun ASLANER for their help in experimental studies.

REFERENCES

[1] S. Glasstone and A. Sesonske, Nuclear Reactor Engineering – Reactor Systems, 4nd ed. Vol.2, Dordrecht, Holland: Springer-Science+Business Media, 1994.

[2] D. Fuloria, N. Kumar, S. Goel, R. Jayaganthan, S. Jha, D. Srivastava, "Tensile Properties and Microstructural Evolution of Zircaloy-4 Processed Through Rolling at Different Temperatures," Materials and Design, vol. 103, pp. 40-51, 2016.

[3] Y. S. Lim, H. G. Kim, Y. H. Jeong, "Experimental Evolution of the Rolling Reduction and Heat-treatment Effects on the Texture and Creep Behavior of a Zircaloy-4 Sheet," Materials Transactions, vol. 49(8), pp. 1922-1925, 2008.

[4] V. Busser, M. C. B. Dubourg, J. Desquines, C. Duriez, J. P. Mardon, "Mechanical Response of Oxidized Zircaloy-4 Cladding Material Submitted to a Ring Compression Test," Journal of Nuclear Materials, vol. 384, pp. 87-95, 2009.

[5] J. S. Yoo, I. S. Kim, "Texture Transformations and Its Role on the Yield Strength of (α+β) Heat Treated Zircaloy-4," Journal of the Korean Nuclear Society, vol. 24(1), pp. 75-85, 1992.
[6] X. Fischer, A. Daidie, B. Eynard, M. Paredes, Research in Interactive Design Vol. 4: Mechanics, Design Engineering and Advanced Manufacturing, Switzerland: Springer International Publishing, 2016.
[7] F. Yılmaz, "Farklı Yöntemlerle Üretilen AB5 Tipi Hidrojen Depolayan Alaşımların Karakterizasyonu," Ph.D. Thesis, Gaziosmanpaşa University, Graduate School of Natural and Applied Sciences, Tokat-Turkey, 2014.
[8] F. Yılmaz, "Nanokristal Al-Si-Sb Alaşımlarının Enerji Yaklaşımı ile Mikromekanik Karakterizasyonu," M.Sc. Thesis, Gaziosmanpaşa University, Graduate School of Natural and Applied Sciences, Tokat-Turkey, 2008.
[9] P. Trivedi, A. K. Patel, R. Maurya, R. Jayaganthan, K. Balani, "Nanomechanical Characterization and Protein Adsorption of Cold-Rolled Zirconium Alloy," The Minerals, Metals & Materials Society, vol. 67(4), pp. 726-732, 2015.
[10] M. Ito, H. Muta, D. Setoyama, M. Uno, S. Yamanaka, "Nanoindentation Studies of High-temperature Oxidized Zircaloy-4 with and without Hydrogen," Journal of Alloys and Compounds, vol. 446-447, pp. 639-642, 2007.
[11] A. H. De Menibus, Q. Auzoux, O. Dieye, P. Berger, S. Bosonnet, E. Foy, V. Macdonald, J. Besson, J. Crepin, "Formation and Characterization of Hydride Blisters in Zircaloy-4 Cladding Tubes," Journal of Nuclear Materials, vol. 449, pp. 132-147, 2014.
[12] G. E. Totten, K. Funatani, L. Xie, Handbook of Metallurgical Process Design, New York: Marcel Dekker Inc., 2004.
[13] W. D. Callister, D. G. Rethwisch, Materials Science and Engineering, SI Version (8th Ed.), New York: John Wiley & Sons Inc., 2011.
[14] D. J.Wulpi, Understanding How Components Fail (3th Ed.),